Rigorous Analysis of the Step Discontinuity in a Planar Dielectric Waveguide

T. E. ROZZI, SENIOR MEMBER, IEEE

Abstract—**Planar dielectric waveguides play an important role in electrooptics and in the submillimeter regions. In many laser configurations and integrated optical components, grooves are etched in the planar surface or overlays are deposited on it. The step is an idealization of such discontinuity. In this paper, the problem of an arbitrary large step under multimode excitation is solved by means of a rigorous variational approach. A rapidly converging expression for the scattering matrix of the step is derived, which is analogous to the one previously derived for transverse discontinuities in closed waveguides. Two choices as to the basis functions are compared: one is constituted by optimally scaled Laguerre functions and the other by the surface waves of both slabs complemented by Laguerre functions. Both the electric field and the magnetic field formulations of the problem have been investigated for the TE case. Numerical results are presented for the scattering matrix of the step under monomode and multimode excitation as well as for its radiation pattern. The accuracy and limitations of existing small step approximations are discussed. The technique is applicable to other transverse discontinuities in open structures.**

I. Introduction

THE STEP in a dielectric slab waveguide is a basic discontinuity occurring in various optical and millimeter wave components, such as distributed feedback lasers, gratings, transformers, antenna feeds, and others. For small steps at the junction of two monomode slabs, a simple and effective approximation has been derived by Marcuse [1]. Clarricoats and Sharpe [2] have applied discrete mode matching to the surface waves at either side of a small step. Hockham and Sharpe [3] have presented a first-order variational solution also valid for small steps. For the problem of arbitrarily large steps, where appreciable coupling takes place between the surface waves and the radiation spectrum, no accurate treatment is available.

Owing to the presence of the continuous spectrum, the method of discrete mode matching is intrinsically ill-suited for dealing with discontinuities in open waveguides. In order to make the continuous spectrum discrete, the use of a Laguerre transform of the wavenumber has been proposed by Mahmoud and Beal [4], without, however, demonstrating the proper convergence of the technique. The introduction of a metallic enclosure, as proposed by Kharadhly [5], is adequate in some respects, but not in others, as, apart from enhanced relative convergence difficulties, this modification alters essentially the boundary condition for radiation, as discussed by Schevchenko [6] and Mittra and Lee [7]. Techniques based on the integral equation approach instead are better suited for this type of problems, as they are capable, in principle, of taking due account of the radiation spectrum and do not suffer from "relative convergence" difficulties. A rigorous technique, based on the Ritz–Galerkin (RG) variational approach, has been developed previously for dealing with discontinuities in closed homogeneous waveguides under multimode excitation [8], [9].

In the present contribution it is shown how the above technique allows a natural extension to the case of open dielectric waveguides, as it makes no essential distinction between discrete and continuous spectrum. The whole spectrum comprises three contributions, the surface waves (discrete), the radiative part of the continuous spectrum, and the reactive part of the continuous spectrum. The first of the three corresponds directly to the propagating modes in a closed waveguide. The last are attenuated in the direction of propagation and represent energy storage in the neighborhood of the discontinuity. The radiative part of the continuous spectrum, however, propagates and represents loss and/or coupling to the surroundings. In the present discussion we will consider the radiation condition to be satisfied.

A consequence of the lossy nature of the problem concerns the convergence of the RG solution. Unlike in the case of a closed, lossless waveguide, the Green's matrix is here symmetric and complex. The extremum property of the solution is consequently replaced by the weaker property of stationarity. This implies that the solution will not converge in a monotonic fashion with increasing order, and also that the electric/magnetic field formulations do not yield upper/lower bounds. However, using a reasonable choice of the expanding functions, the oscillation of the solution decreases rapidly with increasing order, and convergence is rapidly achieved. The electric field and magnetic field formulations of the problem are numerically compared, although a detailed discussion is only given for the latter. Also, two choices of the sequence of expanding functions for the RG procedure are introduced, namely the Laguerre functions with optimally chosen scale factor and the sequence obtained by complementing the surface waves by Laguerre functions. In order to minimize the details, even type TE excitation of a symmetric step is considered. The slab is assumed to be lossless. The extension to asymmetric steps presents no difficulty. The extension to the TM case is nontrivial, but the necessary modifications can be deduced from [10].

Manuscript received August 1, 1977.

The author is with the Philips Research Laboratories, Eindhoven, The Netherlands.

0018-9480/78/1000-0738$00.75 ©1978 IEEE

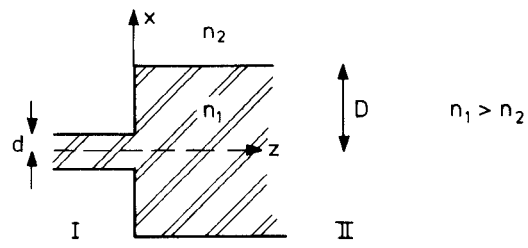

Fig. 1. Step geometry.

II. Waveguide Modes

The longitudinal section of the symmetric slab is shown in Fig. 1. The structure is uniform in the y-direction, not shown. The transverse components of the TE field are E_y and H_x.

A. Surface Waves

After suppressing a propagation factor $e^{j(\omega t-\beta z)}$, these are given by

$$E_{y0}(x)=u(x) \tag{1}$$

$$H_x(x)=-Y_0u(x) \tag{2}$$

with

$$Y_0=\frac{\beta}{\omega\mu_0}=1/Z_0. \tag{3}$$

For symmetric modes in waveguide I, we need only consider $x\geqslant 0$. The scalar function u is given by

$$\begin{aligned} u(x)&=a\cos\kappa x, && x\leqslant d\\ &=a\cos\kappa d e^{-\gamma(x-d)}, && x\geqslant d \end{aligned} \tag{4}$$

where a is a normalization constant and the wavenumbers κ and γ satisfy the eigenvalue equation

$$\kappa\tan\kappa d=\gamma \tag{5}$$

as well as the conservation of the wavenumber

$$\kappa^2+\gamma^2=(n_1^2-n_2^2)k_0^2=v^2 \tag{6}$$

while

$$\beta^2=n_1^2k_0^2-\kappa^2=n_2^2k_0^2+\gamma^2.$$

The normalization constant a is determined by the requirement

$$\int_0^\infty u^2(x)\,dx=1 \tag{7}$$

to be

$$a=\sqrt{\frac{2}{d+1/\gamma}}\ . \tag{8}$$

Analogous expressions hold in guide II, when d is replaced by D.

B. Continuous Spectrum

The continuous spectrum, together with the surface waves, constitutes a complete representation of a physical field in the slab [1], [6]. Again, after suppressing the propagation factor, E_y is given by $E_y=\varphi(x,\rho)$, where

$$\begin{aligned} \varphi(x,\rho)&=\sqrt{\frac{2}{\pi}}\ \frac{1}{C}\cos\sigma x, && x\leqslant d\\ &=\sqrt{\frac{2}{\pi}}\ \cos\left[\rho(x-d)+\alpha\right], && x\geqslant d \end{aligned} \tag{9}$$

where

$$0\leqslant\rho<\infty$$

$$\sigma^2=v^2+\rho^2 \tag{10}$$

$$\alpha=\tan^{-1}\left(\frac{\sigma}{\rho}\tan\sigma d\right), \qquad \left(\lim_{v\to 0}\alpha=\rho d\right) \tag{11}$$

$$C=\left[1+\left(\frac{v}{\rho}\right)^2\sin^2\sigma d\right]^{1/2} \tag{12}$$

while

$$\beta^2=n_1^2k_0^2-\sigma^2=n_2^2k_0^2-\rho^2.$$

The transverse part of the magnetic field is given by $H_x=-\dfrac{1}{Z_0(\rho)}\varphi(x,\rho)$, where

$$\begin{aligned} Z_0&=\frac{\omega\mu_0}{\sqrt{n_2^2k_0^2-\rho^2}}, && \rho<n_2k_0\\ &=\frac{j\omega\mu_0}{\sqrt{\rho^2-n_2^2k_0^2}}, && \rho>n_2k_0. \end{aligned} \tag{13}$$

The normalization is

$$\int_0^\infty dx\,\varphi(x,\rho)\varphi(x,\rho')=\delta(\rho-\rho'). \tag{14}$$

For later use, we note that as $\rho^2\gg v^2$, we have

$$\sigma\to\rho;\quad C\to 1;\quad \alpha\to\rho d \tag{15}$$

$$\varphi(x,\rho)\to\varphi^\infty(x,\rho)=\sqrt{\frac{2}{\pi}}\ \cos\rho x, \qquad 0\leqslant x<\infty \tag{16}$$

i.e., the modes of the continuous spectrum become standing plane waves in a half space, while $\beta\to -j\rho$, with the effect of the dielectric interface having disappeared. Analogous expressions hold for the continuous spectrum $\psi(x,\rho)$ of guide II, after replacement of d by D.

III. Variational Formulation and RG Solution for Surface Wave Incidence

Let us consider the case where n_l surface wave modes are propagating in guide I to the left of the discontinuity and n_r modes in guide II to the right. The discontinuity has then $n_l+n_r=n_i$ "accessible modes" characterized by the functions $\{u_k(x)\colon 1\leqslant k\leqslant n_i\}$. Our aim is to describe the discontinuity as an n_i port, as shown in Fig. 2, by means of its scattering matrix. The electric field amplitudes of the incoming and reflected waves at $z=0$ are expressed by the vectors $\boldsymbol{A},\boldsymbol{B}$, respectively. Let $b(\rho)$ denote the amplitude of the scattered modes of the continuous spectrum in region I and $d(\rho)$ that in region II.

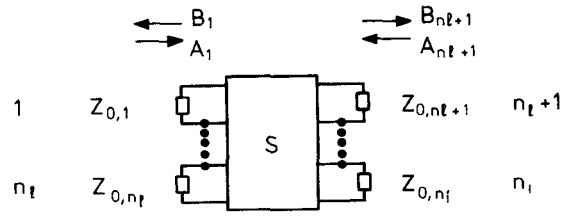

Fig. 2. Schematic multiport representation of the step discontinuity.

Continuity of E_y at $z=0$ is expressed as

$$E_y=\sum_{k=1}^{n_l}(A_k+B_k)u_k(x)+\int_0^\infty d\rho\, b(\rho)Z_0(\rho)\varphi(x,\rho)$$
$$=\sum_{k=n_l+1}^{n_i}(A_k+B_k)u_k(x)+\int_0^\infty d\rho\, d(\rho)Z_0(\rho)\psi(x,\rho). \tag{17}$$

Similarly, the continuity of H_x yields

$$H_x=\sum_{k=1}^{n_l}-\frac{1}{Z_{0k}}(A_k-B_k)u_k(x)+\int_0^\infty d\rho\, b(\rho)\varphi(x,\rho)$$
$$=\sum_{k=n_l+1}^{n_i}-\frac{1}{Z_{0k}}(-A_k+B_k)u_k(x)-\int_0^\infty d\rho\, d(\rho)\psi(x,\rho). \tag{18}$$

The wave amplitudes in (17) can be determined from (18) by multiplying by u_k, φ, ψ in turn, integrating over x, and using orthogonality:

$$b(\rho)=\int_0^\infty \varphi(x,\rho)H_x(x)\,dx \tag{19}$$

$$d(\rho)=-\int_0^\infty \psi(x,\rho)H_x(x)\,dx \tag{20}$$

$$B_k=A_k-s_kZ_{0k}\int_0^\infty dx\,u_k(x)H_x(x) \tag{21}$$

where $s_k=\mp 1$, according to $k\lessgtr n_l$ (left- or right-hand side). Hence, after substituting (19)–(21) in (17) and rearranging, we obtain the integral equation for the magnetic field

$$\sum_{k=1}^{n_i}s_kA_ku_k(x)=\int_0^\infty \mathcal{Z}(x,x')H_x(x')\,dx' \tag{22}$$

with

$$\mathcal{Z}(x,x')=\frac{1}{2}\left\{\sum_{k=1}^{n_i}Z_{0k}u_k(x)u_k(x')\right.$$
$$\left.+\int_0^\infty d\rho\, Z_0(\rho)[\varphi(x,\rho)\varphi(x',\rho)+\psi(x,\rho)\psi(x',\rho)]\right\}. \tag{23}$$

The above is the electric Green's function of the problem in the scattering formulation. Through (21) and (22) a linear relationship is introduced between the amplitude vectors $\boldsymbol{A}$ and $\boldsymbol{B}$. The matrix $\boldsymbol{S}$ such that $\boldsymbol{B}=\boldsymbol{SA}$ is the sought unnormalized scattering matrix. Hence, for $A_l=1$, $A_{k\neq l}=0$, we have $S_{kl}=B_k$. Define

$$h_l\equiv H_x(A_l=1;A_{k\neq l}<0). \tag{24}$$

The magnetic field at the discontinuity can be obtained by superposition:

$$H_x(x)=\sum_{l=1}^{n_i}A_lh_l(x). \tag{25}$$

Under the conditions (24), the integral equation (22) reduces to the set of n_i integral equations

$$s_lu_l(x)=\int_0^\infty dx'\,\mathcal{Z}(x,x')h_l(x'). \tag{26}$$

From a knowledge of the h_l's, the unnormalized scattering matrix can be determined by imposing the port conditions (24) on (21):

$$S_{k,l}=\delta_{k,l}-s_kZ_{0k}\int_0^\infty u_k(x)h_l(x)\,dx. \tag{27}$$

The integral equations (26) cannot yet be solved analytically. Using the RG variational procedure, however, we can approach the solution as closely as desired. Let us introduce first an orthonormal basis $\{L_n(x),\ n=0,\cdots\}$ of "good functions" [11] in the interval $0\leqslant x<\infty$ (in fact, a complete sequence is sufficient). Using this sequence, we can express u_k as

$$u_k(x)=\sum_{n=0}^\infty Q_{nk}L_n(x) \tag{28}$$

with

$$Q_{nk}=\int_0^\infty L_n(x)u_k(x)\,dx. \tag{29}$$

Also we have

$$\varphi(x,\rho)=\sum_{n=0}^\infty P_n(\rho;d)L_n(x) \tag{30}$$

where

$$P_n(\rho;d)=\int_0^\infty dx\,\varphi(x,\rho)L_n(x) \tag{31}$$

$$\psi(x,\rho)=\sum_{n=0}^\infty P_n(\rho;D)L_n(x) \tag{32}$$

where

$$P_n(\rho;D)=\int_0^\infty dx\,\psi(x,\rho)L_n(x) \tag{33}$$

and

$$\mathcal{Z}(x,x')=\sum_{m,n=0}^\infty Z_{mn}L_m(x)L_n(x') \tag{34}$$

with

$$Z_{mn}=\int_0^\infty dx\int_0^\infty dx'\,L_m(x)\mathcal{Z}(x,x')L_n(x')$$
$$=\frac{1}{2}\left\{\sum_k Z_{0k}Q_{mk}Q_{nk}+\int_0^\infty d\rho\, Z_0(\rho)\right.$$
$$\left.\cdot[P_m(\rho;d)P_n(\rho;d)+P_m(\rho;D)P_n(\rho;D)]\right\}. \tag{35}$$

According to (28), (30), (32), and (34), and by means of the sequence of expanding functions (SEF) $\{L_n\}$, the functions $u_k(x)$, $\varphi(x,\rho)$, and $\psi(x,\rho)$ map onto the infinite column vectors $\boldsymbol{Q}_k$, $\boldsymbol{P}(\rho;d)$, $\boldsymbol{P}(\rho;D)$, respectively, whereas the Green's function maps onto the matrix $\boldsymbol{Z}$. The second equation in (35) implies interchanging the order of integration over ρ and x. This is permissible inasmuch as $\mathfrak{L}$ is a distribution and the L_n's are "good functions."

In the RG approach, infinite vectors and matrices are replaced by their finite truncations ($0 \leqslant n \leqslant N$). Hence, the integral equation (26) becomes the finite matrix equation

$$s_l \boldsymbol{Q}_l = \boldsymbol{Z}\boldsymbol{\lambda}_l \tag{36}$$

where the vector $\boldsymbol{\lambda}_l$, stands for the expansion of the unknown function h_l, and from (27), the RG variational expression for the unnormalized scattering matrix of the discontinuity is

$$S_{kl} = \delta_{kl} - s_k s_l Z_{0k} \boldsymbol{Q}_k^T \cdot \boldsymbol{Z}^{-1} \cdot \boldsymbol{Q}_l \tag{37}$$

which is analogous to the expressions for closed waveguides [8] and enjoys variational properties.

Because of the complex nature of the matrix $\boldsymbol{Z}$, however, the exact solution is neither a maximum or a minimum. The normalized scattering matrix is defined for unit resistance terminations at the ports, while the n_i accessible ports of Fig. 2 are closed by the impedances Z_{0k}. In order to pass to the proper impedance normalization, an ideal transformer must be connected at each port. Define

$$\boldsymbol{Z}_0 = \operatorname{diag}(Z_{0k}), \qquad k = 1, \cdots, n \tag{38}$$

then the normalized scattering matrix is given by

$$\bar{\boldsymbol{S}} = \boldsymbol{Z}_0^{-1/2} \cdot \boldsymbol{S} \cdot \boldsymbol{Z}_0^{1/2} \tag{39}$$

or

$$\bar{S}_{kl} = \delta_{kl} - s_k s_l \sqrt{Z_{0k} Z_{0l}}\ \boldsymbol{Q}_k^T \cdot \boldsymbol{Z}^{-1} \cdot \boldsymbol{Q}_l \tag{40}$$

which displays the symmetry required by the reciprocity of the junction. The magnetic field at the discontinuity can be derived from (25) and (36).

A similar analysis can be carried out starting again from (17) and (18) but using the electric field E_y instead of the magnetic field H_x. However, attention now must be paid to the mathematically nontrivial problem of the proper convergence of the integral over ρ. The details are omitted for the sake of brevity.

IV. Scattering of Incident Radiation and Coupling of Surface Waves to the Continuous Spectrum

The preceding formulation is easily extended to the case where radiation is incident on the discontinuity. Consider a real wave packet incident from the left, at $z=0$. This can be expressed in terms of the radiation spectrum for $z<0$.

$$f(x) = \int_0^\infty d\rho\, a(\rho) \varphi(x,\rho). \tag{41}$$

The field can also be expanded as

$$f(x) = \sum_{n=0}^{\infty} f_n L_n(x) \tag{42}$$

where

$$f_n = \int_0^\infty dx f(x) L_n(x) = \int_0^\infty d\rho\, a(\rho) P_n(\rho; d). \tag{43}$$

Owing to orthogonality, it is possible to consider any component of (41) as corresponding to an individual port of a continuous set merging into one "continuous port." Retracing the derivation of the previous section, it is possible to deduce the unnormalized scattering coefficient of a ρ component into the surface waves and of two components, say, ρ and ρ', among themselves. In the magnetic field formulation, these are, respectively,

$$S_{k\rho} = -s_k s_\rho Z_{0\rho} \boldsymbol{Q}_k^T \cdot \boldsymbol{Z}^{-1} \cdot \boldsymbol{P}\left(\rho, \begin{matrix} d \\ D \end{matrix}\right) \cdot (s_\rho = \mp 1 \text{ according as } d \text{ or } D \text{ are chosen}) \tag{44}$$

and

$$S_{\rho,\rho'} = \delta(\rho - \rho') - s_\rho s_{\rho'} \boldsymbol{P}^T\left(\rho; \begin{matrix} d \\ D \end{matrix}\right) \cdot \boldsymbol{Z}^{-1} \cdot \boldsymbol{P}\left(\rho'; \begin{matrix} d \\ D \end{matrix}\right). \tag{45}$$

Unnormalized scattering coefficients are employed so as to avoid the question of complex normalization for imaginary $Z_0(\rho)$.

V. The Discrete Representation

A. Laguerre Functions as an Expanding Set

An appropriate complete set of "good functions" is provided by the normalized Laguerre functions

$$\left\{ L_n(x) = \frac{1}{\sqrt{x_0}} L_n\left(\frac{x}{x_0}\right) e^{-\frac{x}{2x_0}}, \qquad n = 0, 1, 2, \cdots \right\} \tag{46}$$

with

$$\int_0^\infty L_m(x) L_n(x)\, dx = \delta_{mn}. \tag{47}$$

The arbitrary scale parameter x_0 can be adjusted so as to improve convergence, as will be discussed below. The coefficients of the expansions (28), (30), and (32) in terms of the above SEF can be determined analytically and are given in Appendix I. A similar expansion holds for the continuous spectrum in the limit of "lightly trapped waves" (16):

$$\varphi^\infty(x,\rho) = \sum_n P_n^\infty(\rho) L_n(x). \tag{48}$$

The P_n^∞ coefficients are also given in Appendix I.

We shall now proceed to determine the scale parameter x_0 in (46). For a given truncation N of the expansion (28) ($N+1$ is just the order of the variational solution), it is clearly important to be able to represent as closely as possible the accessible modes. If the latter are n_i surface waves, the error function

$$\epsilon_1(x_0)=1-\frac{1}{n_i}\sum_{k=1}^{n_i}\sum_{n=0}^{N}Q_{nk}^2(x_0)>0 \tag{49}$$

gives a measure of the incompleteness of the representation. Requiring ϵ_1 to be a minimum yields an "optimum" value for x_0. The choice of optimization criteria is by no means unique, and other more elaborate approaches involving the continuum have, in fact, been tested, without achieving, however, any significant improvement. The computation of the Green's matrices for the magnetic field formulation in terms of SEF (46) is further discussed in Appendix III.

B. An Alternative SEF

The RG procedure does not require an orthonormal SEF. Completeness is sufficient. In this connection, it is interesting to examine the performance of an alternative complete, nonorthonormal sequence. When the step is excited by a given surface wave, it is reasonable, for small steps, to take the incident surface wave as a trial field, because radiation takes place mainly in the forward direction, and mode mixing is small.

The obvious extension of the argument is to take the n_i surface waves, propagating at *both* sides of the step, as the first n_i functions of the SEF. The sequence is complemented by the Laguerre functions up to the chosen order of the variational solution $\bar{N}$, i.e.,

$$\{g_n: 1\leqslant n\leqslant \bar{N}\}\equiv\{u_1,\cdots,u_{n_i},L_0,\cdots,L_{\bar{N}-n_i-1}\}. \tag{50}$$

Using the above set, straightforward integration yields the amplitudes of the expansion of the surface waves

$$q_{mn}=\int_0^\infty dx\,u_m(x)g_n(x) \tag{51}$$

and that of the continuous spectrum

$$p_n(\rho)=\int_0^\infty \varphi(x,\rho)g_n(x)\,dx \tag{52}$$

$$p_n'(\rho)=\int_0^\infty \psi(x,\rho)g_n(x)\,dx. \tag{53}$$

The above expansions are given explicitly in Appendix II.

The Green's matrix for the magnetic field formulation, analogous to (35), becomes

$$Z_{mn}=\frac{1}{2}\left\{\sum_{k=1}^{n_i}Z_{0k}q_{km}q_{kn}+\int_0^\infty d\rho\,Z_0(\rho)[p_m(\rho)p_n(\rho)+p_m'(\rho)p_n'(\rho)]\right\}. \tag{54}$$

The performance of the above set and of that of Section V-A are compared in Section VII.

The scale parameter x_0 still occurs in (50). Its optimization takes place according to the following criterion. As the surface waves constitute the first n_i functions of the sequence, it is required that the remaining functions $L_0,\cdots,L_{\bar{N}-n_i-1}$ be as close to orthogonal as possible to the former.

VI. Radiation at the Step

The radiation loss of the step can be computed directly from a knowledge of the scattering matrix (40). In terms of the amplitudes of the incoming surface waves, given by the vector $\boldsymbol{A}$ and of the outgoing surface waves (vector $\boldsymbol{B}$) the loss is given by

$$W=\tfrac{1}{2}(\boldsymbol{A}^+\cdot\boldsymbol{Z}_0^{-1}\cdot\boldsymbol{A}-\boldsymbol{B}^+\cdot\boldsymbol{Z}_0^{-1}\cdot\boldsymbol{B}) \tag{55}$$

where + denotes Hermitian conjugation. By means of (18)–(21) and (25), it can be shown that the above expression is identical to that obtained from a consideration of the Poynting vector of the radiation spectrum, which, in turn, is identical to the integral of the power density over the radiative part of the spectrum ($\rho<n_2k_0$).

The computation of the far field is based on a saddle point evaluation of the far field in each half-space. From (9) and (17) and in account of the even parity with respect to ρ, the y-component of the electric field of the continuum spectrum can be written as

$$E_y^R(x,z)=\frac{\omega\mu_0}{\sqrt{2\pi}}\int_{-\infty}^{+\infty}d\rho\frac{d(\rho)}{\beta(\rho)}e^{-j[\rho(x-d)+\alpha(\rho)+\beta z]}. \tag{56}$$

Passing to polar coordinates,

$$x=r\sin\theta,\quad z=r\cos\theta$$

$$\rho=n_2k_0\sin w,\quad \beta=n_2k_0\cos w \tag{57}$$

(56) becomes

$$E_y^R(x,z)=\frac{\omega\mu_0}{\sqrt{2\pi}}\int_{-\frac{\pi}{2}-j\infty}^{\frac{\pi}{2}+j\infty}dw f(w)e^{-jrn_2k_0\cos(w-\theta)} \tag{58}$$

where

$$f(w)=d(n_2K_0\sin w)e^{-j[\alpha(w)-n_2k_0d\sin w]}. \tag{59}$$

In the limit $k_0r\gg1$, the far field can be evaluated by the saddle-point method after deforming the integration path in the complex w-plane into a steepest descent contour (SDC), as described in [12, pp. 459–470] and [6, pp. 108–112]. Care, however, must be taken that in deforming the contour no singularity is crossed in the w-plane. These are of two kinds: branch lines or poles (improper modes). The former kind occurs at $w=\pm\pi/2$, where $d\rho/dw=0$. Hence we must keep $|\theta|<\pi/2$. Poles corresponding to improper modes are crossed for θ smaller than some critical angle. In the same interval of angles, however, the improper modes make no contribution to the radiation field, as their field tends exponentially to zero for increasing r. The far field outside the slab is then given by

$$E_y^R(r,\theta)/\omega\mu_0\cong\sqrt{\frac{1}{n_2k_0r}}\,f(\theta)e^{-j\left(rn_2k_0-\frac{\pi}{4}\right)} \tag{60}$$

and the radiation pattern is proportional to $|d|^2$, i.e., the spectral power density of the radiation modes. Analogous considerations hold for $z<0$.

TABLE I
SCATTERING MATRIX OF STEP BETWEEN MONOMODE SLABS—ORTHONORMAL BASIS OF SECTION V-A: MAGNETIC FIELD FORMULATION; $d/D=0.2$, $n_2k_0D=1$, $vD=2$

N	$\lvert\Gamma_1\rvert$%	$\sphericalangle\Gamma_1-\pi$(RAD)	$\lvert T\rvert$%	$\sphericalangle T$	$\lvert\Gamma_2\rvert$%	$\sphericalangle\Gamma_2$	RAD LOSS%
0	20.88	-.0865	94.22	-.0149	26.55	.0413	6.87
1	20.77	-.0920	93.77	-.0135	25.28	.0540	7.77
2	20.72	-.1038	93.70	-.0099	24.73	.0532	7.92
3	20.49	-.0802	94.10	-.0096	24.82	.0648	7.25
4	20.36	-.0832	94.14	-.0082	24.83	.0737	7.13
5	20.41	-.0859	94.15	-.0076	24.79	.0759	7.19
6	20.40	-.0858	94.15	-.0076	24.78	.0759	7.19
7	20.40	-.0858	94.16	-.0075	24.79	.0763	7.18
8	20.40	-.0860	94.16	-.0075	24.79	.0764	7.18
20	20.40	-.0860	94.16	-.0075	24.79	.0764	7.18

TABLE II
SCATTERING MATRIX OF STEP BETWEEN MONOMODE SLABS—ORTHONORMAL BASIS OF SECTION V-B: ELECTRIC FIELD FORMULATION; $d/D=0.2$, $n_2k_0D=1$, $vD=2$

N	$\lvert\Gamma_1\rvert$%	$\sphericalangle\Gamma_1-\pi$(RAD)	$\lvert T\rvert$%	$\sphericalangle T$	$\lvert\Gamma_2\rvert$%	$\sphericalangle\Gamma_2$	RAD LOSS%
0	22.56	-.0704	96.99	.0205	21.50	.1159	0.83
1	19.66	-.0593	94.52	.0055	23.24	.1813	6.80
2	20.35	-.0868	93.78	-.0153	25.05	.0832	7.92
3	20.52	-.0640	94.35	-.0018	24.51	.0610	6.72
4	20.28	-.0698	94.10	-.0038	24.80	.0663	7.34
5	20.69	-.0923	94.44	-.0084	24.52	.0866	6.53
6	20.14	-.0771	93.91	-.0059	25.02	.0763	7.76
7	20.45	-.1001	94.22	-.0103	24.72	.0879	7.05
8	20.33	-.0738	94.07	-.0050	24.88	.0693	7.37

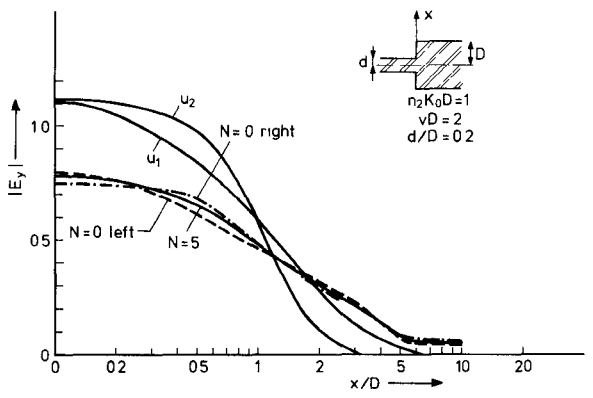

Fig. 3. Transverse electric field at discontinuity $n_2k_0D=1$, $vD=2$, $d/D=0.2$.

TABLE III
SCATTERING MATRIX OF STEP BETWEEN MONOMODE SLABS—NONORTHONORMAL BASIS OF SECTION VI: MAGNETIC FIELD FORMULATION; $d/D=0.2$, $n_2k_0D=1$; $(n_1^2-n_2^2)k_0^2D^2=4$

N	$\lvert\Gamma_1\rvert$%	$\sphericalangle\Gamma_1-\pi$(RAD)	$\lvert T\rvert$	$\sphericalangle T$	$\lvert\Gamma_2\rvert$%	$\sphericalangle\Gamma_2$	RAD LOSS%
0	19.68	-.1282	91.33	-.0210	30.27	.0485	12.7
1	20.54	-.0779	93.92	-.0097	24.43	.0650	7.57
2	20.61	-.0840	93.87	-.0084	24.39	.0697	7.64
3	20.42	-.0825	94.13	-.0086	24.76	.0703	7.22
4	20.39	-.0835	94.17	-.0083	24.81	.0722	7.16
5	20.39	-.0862	94.16	-.0074	24.79	.0765	7.18
6	20.40	-.0861	94.16	-.0075	24.78	.0764	7.18
7	20.40	-.0862	94.16	-.0074	24.78	.0766	7.19
8	20.40	-.0861	94.16	-.0075	24.79	.0765	7.18

VII. EXAMPLES AND NUMERICAL RESULTS

A. Accuracy Tests and Convergence of the Variational Solution

The results of a convergence test for a large step discontinuity are presented in Table I. For the choice of the parameters in the table, both slabs are single moded. The radiation losses refer to incidence from the left. The radiation losses for incidence from the right are easily deduced from these data. For $N=8$, all the above quantities, which completely characterize the junction, have reached their convergence values within four significant figures. For the sake of comparison, the same quantities were computed using the same basis but in the electric field formulation. The results are shown in Table II. As expected, from the distributional character of the Green's function, the convergence is slower in this formulation. On account of this, all the following results were computed using the magnetic field formulation.

It is also interesting to carry out the same computation utilizing the complete, but not orthonormal basis discussed in Section V-B. The results are shown in Table III. In particular, $N=0$ means that the discontinuity field is assumed to be that of the incoming surface wave. This commonly used approximation is inadequate for sizeable steps. A considerably better approximation is provided by assuming the discontinuity field to be a linear combination of the incident and transmitted surface waves ($N=1$). For $N=6$, the results are virtually identical to those of Table I, considering the finite accuracy of the numerical computation.

The set of Section V-A will be employed in the following examples. The last test consisted in checking how well the continuity of E_y at $z=0$, as expressed by (17), was satisfied by a given variational solution of the integral equation (22) for H_x. In Fig. 3 the moduli of E_y at either side of the step are plotted versus x/D for $N=0.5$. In the latter case, the two curves are no longer distinguishable. For reference, the surface wave fields u_1, u_2 are also plotted.

B. Examples

The variation of the scattering matrix of the step for varying width of the smaller guide d is illustrated in Figs. 4 and 5. Fig. 4 shows the moduli of the reflection and transmission coefficients, as well as the radiation losses of the step. Since this example refers to fairly high refractive slabs in air, radiation losses are low for less than sizeable steps. Up to moderate steps ($d/D \gtrsim 0.5$), for the present values of the parameters, the moduli of the reflection coefficients for incidence from the left (Γ_1) and from the right (Γ_2) are virtually identical. Their value is closely approximated by the reflection coefficient of an ideal admittance step without mode conversion

$$\Gamma_2=-\Gamma_1=\frac{\beta_1-\beta_2}{\beta_1+\beta_2}. \tag{61}$$

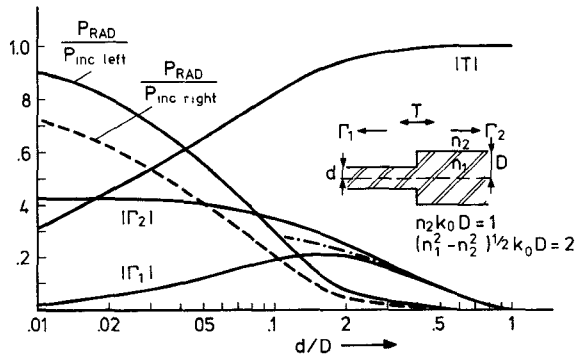

Fig. 4. Amplitudes of the reflection and transmission coefficients of a step between monomode slabs and radiation losses versus step height $N=5$, $n_2k_0D=1$, $vD=2$.

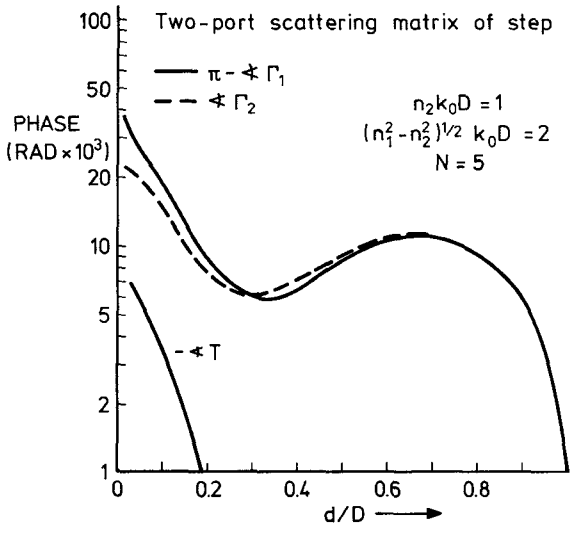

Fig. 5. Phases of the reflection and transmission coefficients of the step of Fig. 4.

As d decreases, $|\Gamma_2|$ keeps increasing in excess of the above approximation up to its limiting value, the reflection from a semi-infinite slab. $|\Gamma_1|$ keeps increasing below (61). Then, after going though a maximum, it goes to zero, as it should, since the surface wave is no longer guided for $d=0$. The transmission coefficient also decreases for increasing step size, since the energy increasingly leaks out in the form of radiation, as can be seen from the plots of the radiation loss.

The argument of the reflection coefficent, given in Fig. 5, is not negligible, even for small steps. It is noteworthy that in the region where the phase goes through two turning points, the accurate variational solution predicts a sizeable deviation of the modulus of the transmission coefficient from the "mode projection" approximation of [1], which is otherwise quite fair, even for large steps. The phase of the transmission coefficient is rather small, in this case less than 0.01 rad. The angular dependence of the radiation pattern is illustrated in Fig. 6 for $N=0$, 5, 8. Unit incidence from the left is assumed. While the only peak is indeed forward, backscattered radiation is not negligible.

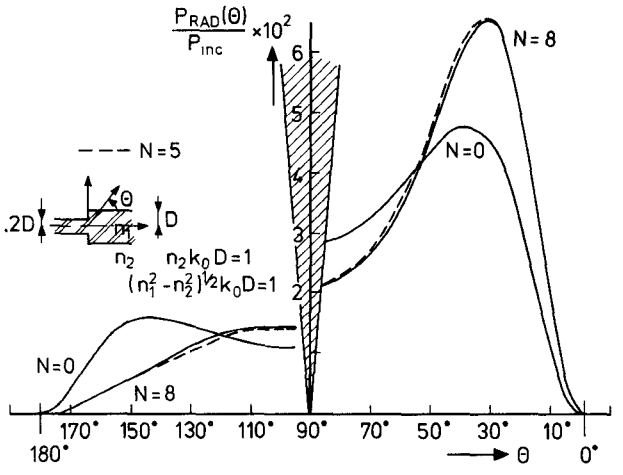

Fig. 6. Convergence of the radiation pattern (incidence from left) for increasing order of the variational solution $n_2k_0D=1$, $vD=2$.

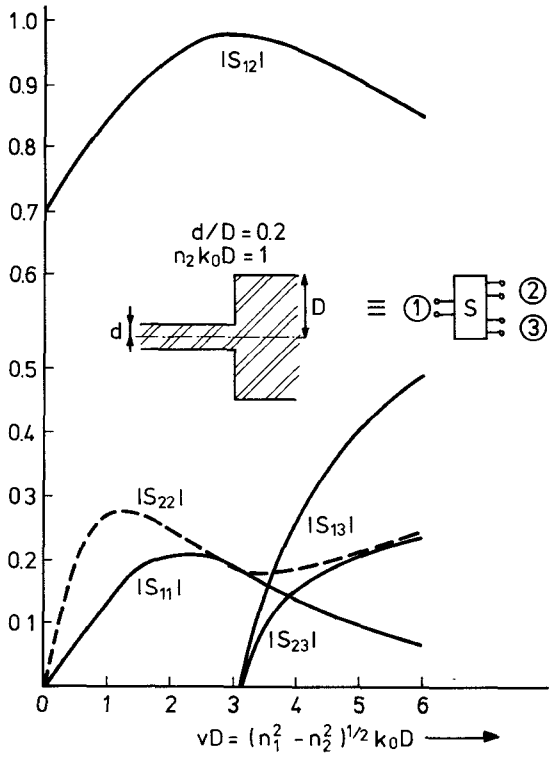

Fig. 7. Amplitude of the elements of the scattering matrix of a multimode step versus vD, $n_2k_0D=1$, $N=5$.

The behavior of the step discontinuity under multimode excitation is illustrated in Fig. 7, where the moduli of the elements of the scattering matrix are plotted versus the "normalized frequency" $vD=(n_1^2-n_2^2)^{1/2}k_0D$. As v increases beyond $vD=\pi$, the thicker slab allows two modes to propagate, whereas the thinner slab remains monomode. Even before the cutoff value is reached, the imminent presence of the second mode is felt, as shown by the inflection of $|S_{11}|$ and $|S_{12}|$ for incidence from the left (port 1). This is accompanied by increasing radiation losses. Similar features reappear around $vD=2\pi$, where a third mode can propagate in the thicker slab.

VIII. Conclusion

The scattering of TE modes by a symmetric step discontinuity in a planar dielectric waveguide has been treated by means of a rigorous variational solution. Two sequences of expanding functions have been investigated. The numerical examples demonstrate that rapid convergence is achieved, using either of the two choices when adopting a magnetic field formulation. Results are presented on the scattering of surface waves for varying step ratio and "normalized" frequency. Also the limitations of small step approximations, particularly with regard to phase and radiation properties, are illustrated.

In particular, the results on the radiation characteristics show that backward radiation cannot be neglected for sizeable steps. An accurate analysis like the one presented becomes mandatory when dealing with large steps, with multiple interacting steps, even if the steps are moderate, or with multiple surface wave excitation. The extension to asymmetric steps presents no difficulty. The same technique can also be applied to other important discontinuities in dielectric waveguides.

Appendix I
The Coefficients P_n and Q_n of Section V-A

From [12, pp. 92, 844, and 1037], after some algebra, we obtain

$$P_n^{\infty}(\rho)=\sqrt{\frac{2x_0}{\pi}}\,(-1)^n\frac{\cos\left[(2n+1)\tan^{-1}2\rho x_0\right]}{\left(\frac{1}{4}+\rho_0^2x^2\right)^{1/2}} \tag{A1}$$

$$Q_n=a\sqrt{x_0}\left\{(-1)^n\frac{\cos\left[(2n+1)\tan^{-1}2\kappa x_0\right]}{\left(\frac{1}{4}+\kappa^2x_0^2\right)^{1/2}}+\sum_{k=0}^{n}(-1)^k e^{-\frac{d}{2x_0}}L_{n-k}^{k}\left(\frac{d}{x_0}\right)\cdot\left[\frac{\cos\kappa d}{\left(\frac{1}{2}+\gamma x_0\right)^{k+1}}-\frac{\cos\left[(k+1)\tan^{-1}2\kappa x_0+\kappa d\right]}{\left(\frac{1}{4}+\kappa^2x_0^2\right)^{(k+1)/2}}\right]\right\} \tag{A2}$$

$$P_n(\rho;d)=\sqrt{\frac{2x_0}{\pi}}\left[\frac{(-1)^n}{C}\frac{\cos(2n+1)\tan^{-1}2\sigma x_0}{\left(\frac{1}{4}+\sigma^2x_0^2\right)^{1/2}}+\sum_{k=0}^{n}(-1)^k e^{-\frac{d}{2x_0}}L_{n-k}^{k}\left(\frac{d}{x_0}\right)\left\{\frac{\cos\left[(k+1)\tan^{-1}2\rho x_0+\alpha\right]}{\left(\frac{1}{4}+\rho^2x_0^2\right)^{(k+1)/2}}-\frac{1}{C}\frac{\cos\left[(k+1)\tan^{-1}2\sigma x_0+\sigma d\right]}{\left(\frac{1}{4}+\sigma^2x_0^2\right)^{(k+1)/2}}\right\}\right]. \tag{A3}$$

The finite sum in (A3) goes rapidly to zero for increasing so that for $\rho^2\gg v^2$, (A3) reduces to (A1).

Appendix II
The Coefficients q, p, p', of Section V-B

The elements of the expansion in terms of the set of Section V-B are

$$\begin{aligned}
q_{mn}&=\delta_{m,n}, \qquad 1\leqslant m\leqslant n_l, \quad 1\leqslant n\leqslant n_l\\
&=a_m a_n\frac{1}{2}\left[\frac{\sin(\kappa_m+\kappa_n)d}{\kappa_m+\kappa_n}+\frac{\sin(\kappa_m-\kappa_n)d}{\kappa_m-\kappa_n}\right]\\
&\quad+\frac{\cos\kappa_m d}{\gamma_m^2+\kappa_n^2}\left[e^{\gamma_m(d-D)}(-\gamma_m\cos\kappa_n D+\kappa_n\sin\kappa_n D)\right.\\
&\quad\left.+\gamma_m\cos(\kappa_n d)-\kappa_n\sin\kappa_n d\right]\\
&\quad+\frac{\cos\kappa_m d\cdot\cos\kappa_n D}{\gamma_m+\gamma_n}e^{\gamma_m(d-D)}\Bigg\},\\
&\qquad 1\leqslant m<n_l \quad n_l<n\leqslant n_i\\
&=\begin{cases}Q_{m,n-n_l-1}, & 1\leqslant m\leqslant n_l, \quad n_l<n\leqslant\bar{N}\\ \delta_{mn}, & n_l<m\leqslant n_i, \quad 1\leqslant n\leqslant n_l\\ q_{n,m-1}, & n_l<m\leqslant n_i, \quad n_l<n\leqslant n_i\end{cases}\\
p_n(\rho)&=0, \qquad 1\leqslant n\leqslant n_l\\
&=\frac{a_n}{\sqrt{2\pi}}\frac{1}{C(\rho,d)}\left[\frac{\sin(\kappa_n+\sigma)d}{\kappa_n+\sigma}+\frac{\sin(\kappa_n-\sigma)d}{\kappa_n-\sigma}\right]\\
&\quad+\frac{1}{\kappa_n+\rho}\left[\sin((\kappa_n+\rho)D+\vartheta(\rho,d))\right.\\
&\quad\left.-\sin(\kappa_n d+\alpha(\rho,d))\right]\\
&\quad+\frac{\cos\vartheta(\rho,d)}{\rho-\kappa_n}\left[\sin(\rho-\kappa_n)D-\sin(\rho-\kappa_n)d\right]\\
&\quad+\frac{2\cos\kappa_n D}{\gamma_n^2+\rho^2}\left[\gamma_n\cos(\vartheta(\rho,d)+\rho D)\right.\\
&\quad\left.-\rho\sin(\vartheta(\rho,d)+\rho D)\right]\\
&\quad-\frac{2\sin\vartheta(\rho,d)}{\rho-\kappa_n}\sin\left[(\rho-\kappa_n)\frac{d+D}{2}\right]\\
&\quad\cdot\sin\left[(\rho-\kappa_n)\frac{D-d}{2}\right]\Bigg\},\\
&\qquad n_l<n\leqslant n_i
\end{aligned} \tag{A4}$$

where $(\vartheta(\rho,d)=\alpha(\rho,d)-\rho d)$.

$$P_n(\rho)=P_{n-n_l-1}(\rho,d), \qquad n_i<n\leqslant\bar{N}. \tag{A5}$$

$$P_n(\rho)=\frac{a_n}{\sqrt{2\pi}}\left\{\frac{1}{C(\rho,D)}\left[\frac{\sin(\kappa_n+\sigma)d}{\kappa_n+\sigma}+\frac{\sin(\kappa_n-\sigma)d}{\kappa_n-\sigma}\right]\right.$$
$$+\frac{2\cos\kappa_n d}{C(\rho,D)}\frac{1}{\gamma_n^2+\sigma^2}\left[e^{\gamma_n(d-D)}(\sigma\sin\sigma D-\gamma_n\cos\sigma D)\right.$$
$$\left.-(\sigma\sin\sigma d-\gamma_n\cos\sigma d)\right]+\frac{2\cos\kappa_n d}{\gamma_n^2+\rho^2}\rho^{\gamma_n(d-D)}$$
$$\left.[\gamma_n\cos\alpha(\rho,D)-\rho\sin\alpha(\rho,D)]\right\},\qquad 1\leqslant n\leqslant n_l$$
$$=\begin{cases}0, & n_l<n\leqslant n_i\\ P_{n-n_i-1}(\rho,D), & n_i<n\leqslant N.\end{cases}\tag{A6}$$

Appendix III
Computation of the Green's Matrix

The computation of the Green matrices (35) requires integration over an infinite interval. It is advantageous to extract analytically the contribution of the integral for large values of ρ. For the sake of compactness, define

$$I_{mn}(\rho)=P_m(\rho;d)P_n(\rho;d)+P_m(\rho;D)P_n(\rho;D).\tag{A7}$$

Let $\boldsymbol{Z}^r$ denote the contribution of the continuous spectrum in (35)

$$2Z^r_{mn}=\omega\mu_0\int_0^{n_2k_0}\frac{I_{mn}(\rho)}{\sqrt{n_2^2k_0^2-\rho^2}}\,d\rho$$
$$+j\omega\mu_0\int_{n_2k_0}^{\rho_0}\frac{I_{mn}(\rho)\,d\rho}{\sqrt{\rho^2-n_2^2k_0^2}}+j\omega\mu_0L_{mn}\tag{A8}$$

where $\rho_0\gg\max(n_2k_0,v)$. The first integral represents the contribution of the radiative part of the continuous spectrum. The second integral and the last term represent the contribution of the reactive part of the continuous spectrum. The last term, in particular, is a purely inductive asymptotic contribution. Noting that $\boldsymbol{P}(\rho;d)$, $\boldsymbol{P}(\rho;D)\to\boldsymbol{P}^\infty(\rho)$ as $\rho^2\gg v^2$, we have

$$L_{mn}=2\int_{\rho_0}^{\infty}\frac{P_m^\infty(\rho)P_n^\infty(\rho)}{\rho}\,d\rho.\tag{A9}$$

The above integral can be evaluated (thanks to [12, p. 143]) and the result is

$$L_{mn}=\frac{4}{\pi}(-1)^{m+n}x_0\left[\sum_{k=1}^{|m-n|}b_k+\sum_{k=1}^{m+n}b_k+\sum_{k=1}^{|m-n|-1}b_k\right.$$
$$\left.+\sum_{k=1}^{m+n+1}b_k+4\ln\operatorname{cosec}\varphi_0\right]\tag{A10}$$

where

$$\varphi_0=\tan^{-1}2\rho_0x_0\tag{A11}$$
$$b_k=\frac{1}{k}\left[(-1)^k-\cos 2k\varphi_0\right].\tag{A12}$$

The singularity in (A.5) is eliminated (and the computational efficiency improved) by setting:

$$\rho=n_2k_0\sin t,\qquad \rho\leqslant n_2k_0$$
$$=n_2k_0\cosh t,\qquad \rho\geqslant n_2k_0.\tag{A13}$$

Acknowledgment

The author is indebted to Prof. R. Mittra and to Dr. T. Itoh for some clarifying discussions at the early stages of this research. The contributions of G. in 't Veld, who carried out the numerical computations, and of all the colleagues who improved the manuscript with their constructive criticism, in particular Prof. A. T. de Hoop (on leave of absence from the Delft University of Technology) and Dr. C. Velzel, also are gratefully acknowledged.

References

[1] D. Marcuse, "Radiation losses of tapered dielectric slab waveguides," *Bell Syst. Tech. J.*, vol. 49, pp. 273–287, Feb. 1970.
[2] P. Clarricoats and A. Sharpe, "Modal matching applied to a discontinuity in a planar surface waveguide," *Electron. Lett.*, vol. 8, pp. 28–29, Jan. 1972.
[3] G. A. Hockham and A. B. Sharpe, "Dielectric waveguide discontinuities," *Electron. Lett.*, vol. 8, pp. 230–231, May 1972.
[4] S. Mahmoud and J. Beal, "Scattering of surface waves at a dielectric discontinuity on a planar waveguide," *IEEE Trans. Microwave Theory Tech.*, vol. MTT-23, pp. 193–198, Feb. 1975.
[5] C. Brooke and M. Kharadhly, "Step discontinuities on dielectric waveguides," *Electron. Lett.*, vol. 12, pp. 471–473, Sept. 1976.
[6] V. Schevchenko, *Continuous Transisions in Open Waveguides*. Golem, 1971.
[7] R. Mittra and S. Lee, *Analytical Techniques in the Theory of Guided Waves*. New York: McMillan, 1971.
[8] T. Rozzi, "Network analysis of strongly coupled transverse apertures in waveguides," *Intl. J. Circuit Theory Appl.*, vol. 1, pp. 161–178, June 1973.
[9] T. Rozzi and W. Mecklenbräuker, "Wideband network modelling of interesting inductive irises and steps," *IEEE Trans. Microwave Theory Tech.*, vol. MTT-23, pp. 235–245, Feb. 1975.
[10] T. Rozzi, "Accurate analysis of the near field of d.h. lasers," to be published.
[11] M. Lighthill, *Generalized Functions and Fourier Transforms*. New York: Cambridge, 1962.
[12] L. Felsen and N. Marcuvitz, *Radiation and Scattering of Waves*. Englewood Cliffs, NJ: Prentice Hall, 1973.
[13] I. Gradshteyn and I. Ryzhik, *Table of Integrals Series and Products*. New York: Academic Press, 1965.